Modelling of hydrogen induced pressurization of internal cavities

Jean-Gabriel Sezgin, Cédric Bosch, Aurore Montouchet, Gilles Perrin, Krzysztof Wolski

▶ **To cite this version:**

Jean-Gabriel Sezgin, Cédric Bosch, Aurore Montouchet, Gilles Perrin, Krzysztof Wolski. Modelling of hydrogen induced pressurization of internal cavities. International Journal of Hydrogen Energy, 2017, 42 (22), pp.15403-15414. 10.1016/j.ijhydene.2017.04.106 . emse-01578818

HAL Id: emse-01578818

https://hal-emse.ccsd.cnrs.fr/emse-01578818v1

Submitted on 29 Oct 2022

HAL is a multi-disciplinary open access archive for the deposit and dissemination of scientific research documents, whether they are published or not. The documents may come from teaching and research institutions in France or abroad, or from public or private research centers.

L'archive ouverte pluridisciplinaire **HAL**, est destinée au dépôt et à la diffusion de documents scientifiques de niveau recherche, publiés ou non, émanant des établissements d'enseignement et de recherche français ou étrangers, des laboratoires publics ou privés.

Distributed under a Creative Commons Attribution - NonCommercial 4.0 International License

Modelling of hydrogen induced pressurization of internal cavities

Jean-Gabriel Sezgin [a,c,*], C edric Bosch [a], Aurore Montouchet [b], Gilles Perrin [c], Krzysztof Wolski [a]

[a] Centre SMS, CNRS UMR 5307 LGF, Ecole des Mines de Saint Etienne, France
[b] AREVA Creusot Forge, Le Creusot, France
[c] AREVA NP, Paris, France

Internal cavities can constitute a crack initiation site especially if filled with hydrogen at high pressure. A new refined equation of state based on recent NIST database has been introduced in order to model the equilibrium pressure. It is based on a thermodynamic definition of fugacity and uses the NIST data relating hydrogen density and pressure to define a new fugacity pressure quadratic dependence. The resulting Equation Of State (EOS) is compared to the standard Abel–Noble EOS and it is shown that for a given fugacity, imposed by a Sievert's law, the corresponding pressure is significantly higher. This new refined EOS was introduced into a previously developed numerical model of hydrogen diffusion and desorption and applied to evaluate the kinetics of pressure build-up within a cavity and its equilibrium pressure. It has been shown that the kinetics of pressure build-up at room temperature, which reaches values close to equilibrium in some hundreds of hours, is compatible with the industrial quality control procedures. The calculated pres-sures are in the range 4500–8650 bars depending on hydrogen solubility, which differs between the matrix and the segregation bands, and tend to equilibrium values obtained from mass balance approach.

Introduction

Substantial efforts have been put on the investigation of environmentally assisted fracture during the last decades mainly in order to prevent the premature failure of structures. Structure optimization and safety criteria imply better knowledge of hydrogen embrittlement mechanisms of metallic alloys, especially for low alloy steels. Several mechanisms of hydrogen embrittlement are available in literature [1] mostly based on reduction of energy required to create crystallographic defects (*e.g.* dislocations, vacancies, micro-voids…), energy related to defects mobility [2–4] or surface and cohesion energy [5,6]. Hydrogen in solution may have several origins mainly linked to manufacturing process or operating conditions. A distinction has been made between the internal hydrogen typically issued from manufacturing process, namely from ingot solidification step and the external hydrogen, typically issued from 'in service'

* *Corresponding author*. Ecole des Mines de Saint-Etienne, 158 Cours Fauriel – CS 62362, 42023 Saint-Etienne Cedex 2, France. Fax: +33 4 77 42 00 00.
E-mail address: jean-gabriel.sezgin@mines-stetienne.fr (J.-G. Sezgin).

electrochemical reactions [7–10]. Hydrogen Induced Cracking (HIC) could be observed either at the end of manufacturing process or during service in highly hydrogenated conditions [11,12]. HIC phenomena may be considered as a transverse field involving mechanisms of hydrogen embrittlement (*e.g.* modification of mechanical properties by hydrogen in solution [13–15]) and pressurization of cavities [16,17]. Since the effective pressure within the cavity cannot be measured through experimental procedure, a relevant model of diffusion-desorption has to be used to be predictive regarding blistering or manufacturing process, in conformity with regulations guidelines [18].

Depending on the metallurgical state of the material, cavities of different sizes and shapes can by observed. The smallest, almost spherical, in the range of some nanometers, can only be identified by TEM as this is the case for austenitic stainless steel exposed to irradiation in nuclear industry [19]. The largest, frequently flat and called penny-shaped with the diameter up to dozens of millimeters and thickness in the range of several microns, are easily visible on polished cross-sections by standard optical or scanning electron microscopies, typically 'blisters' in rolled carbon or microalloyed steels exposed to high hydrogen fugacity media in oil&gas industry. In between, cavities can also form at the interface with individual MnS inclusions where the difference between thermal expansion coefficients of MnS [20] (16.10^{-6} K^{-1}) and ferritic steels [21] (12.10^{-6} K^{-1}) can result in decohesions. For a typical size of MnS of 5 microns, cooling from 1000 °C down to room temperature would result in decohesion of 20 nm. In forged components MnS inclusions form flat colonies within the mesoscopic areas of high concentration of alloying elements, called microsegregations. The diameter of such colonies is typically of the order of some hundreds of microns and can reach a millimeter range. Moreover, in association with 20 nm decohesion on each individual decohesion, such a colony can be considered as initial penny-shaped compliant volume.

To estimate the pressure build-up in these "penny shaped" volumes, a modelling procedure has to be conducted. Some models to predict the formation of such defects have already been proposed in the literature [22–25] although they could not be effectively used. Actually, these models present some limits mainly due to the unrealistic pressures within the cavity which are due to the use of the ideal gas behavior of hydrogen leading to an equilibrium pressure in the range of GPa. Additionally, the assumed homogeneity of the alloy [23] or the continuous approach to handle with cavities [24] equally distributed in the shell instead of being located at the mid wall thickness, constitute secondary limitations. Consequently, the diffusion and desorption of hydrogen into the cavity together with the estimation of the transient redistribution of hydrogen and resulting pressure build up within the cavity during the thermal treatment will be solved by using the model proposed in Ref. [26] which better fits the present context. This model based on Finite Difference Method has been proposed in order to estimate the transient redistribution of hydrogen in heavy components such as pressure vessels. An approach has also been proposed to treat the solid–gas interface (corresponding to the alloy–cavity interface) and the matrix-segregation interface (generated by intrinsic composition heterogeneities linked to manufacturing process of heavy components). To handle the desorption step at the solid–gas interface; it is assumed that hydrogen is in thermodynamic equilibrium which is expressed by adequate fugacity in Sievert's law.

In this paper, the hydrogen induced pressurization of cavities will be assessed in accordance with the conditions of industrial manufacturing of heavy components. These pressurized cavities have triggered a considerable interest of both Oil & Gas (*e.g.* blistering) and nuclear industry (*e.g.* HIC at the end of industrial process) and particularly in Europe where similar problematic has resulted in the temporary shut-down of two reactors in Belgium [18]. The study will then be based on the feedback of a scrapped pressurized vessel shell aimed to compose a steam generator. Such shells are composed of 16MND5 through 20MnNiMo5 grades (also called 16-20MND5), a low alloy steel which exhibits some heterogeneities. The composition heterogeneities are a consequence of thermal kinetics during solidification (*i.e.* solutal and thermal convection in plain or hollow ingots) [33–36]. Since the pressure assessment will be modeled at a component scale, it is considered that the macroscopic heterogeneities are located at mid thickness in the radial direction. It is also considered that the preexisting cavity is generated after forging by a previous cooling step. It is assumed, as demonstrated above, that the difference in thermal expansion coefficients between MnS and alloy has led to non-coherent interfaces on which the recombination of hydrogen according to Sievert's equilibrium is possible.

The first objective of this paper is then to propose a refined and effective description of hydrogen considered as a real gas under high pressures. This point consists in clarifying the behavior of high pressure hydrogen considered as a real gas in the expected temperature range. The second objective is to elucidate the pressure build-up within a cavity (*e.g.* generated by the non-coherent steel-MnS interface) during heat treatment in the aforementioned heterogeneous pressurized vessel shell composed of low alloy steel (industrial 16-20MND5 grades).

To reach these objectives, an alternative approach to define hydrogen fugacity has been proposed after recalling description available in literature. This formulation allows an accurate description of dihydrogen up to 20 kbar under usual manufacturing conditions. This approach is then correlated to the typical industrial thermal cycle to elucidate the maximal expected pressure reachable in aforesaid context by using the diffusion-desorption procedure proposed in Ref. [26]. The related kinetic effects caused by mass diffusion and leading to a dynamic redistribution of hydrogen within the component during cooling will also be analyzed.

Previous work related to real gas description of hydrogen

Preliminary simulations of diffusion and desorption of hydrogen using an ideal gas behavior for hydrogen in cavity have led to unrealistically high pressures in GPa range [22,27]. The Equation Of State (EOS) is therefore a key parameter to provide an accurate estimation of the pressure build-up

within cavities. The aforementioned models present the specificity of treating hydrogen as a real gas in similar pressure and temperature range. In addition, investigations on gaseous hydrogen behavior have mainly been developed for cryogenic vessel applications. Consequently, some thermodynamic properties involved in cavity pressurization studies are not always properly used or are considered even if they are not relevant in the considered temperature range, namely, evaluated at the critical point (P_c; T_c; ρ_c) defined by (13.1 bar;33.20 K;31.4 kg m^{-3}) which is out of the range regarding any manufacturing processes encountered in the industry [25,28].

Several Equations Of States (EOS) are available in literature and applicable to hydrogen gas. Some of these EOS are widespread for hydrogen behavior and may be used in diverse fields such as material science [29], cryogenics [30] or ballistics [31]. The EOS laws considered in this paper are the following: ideal gas, Abel–Noble [29], Van-der-Waals [30], Hemmes [32]. It is noteworthy that all these equations correspond to a given application range regarding pressure and temperature. As an example, the EOS proposed by Hemmes is applicable for temperatures from 100 K to 1000 K and pressures up to 10^6 bar. Generally, these EOS are to be implemented in either analytical or numerical models which result in a constraint on its implementation, in particular, instabilities in simulations have to be avoided. To quantify the differences between ideal gas model and real gas models, a compressibility factor is usually defined as $Z = \frac{pv}{RT}$, where p represents the pressure, v the molar volume, R the gas constant and T the temperature. Two groups of EOS can be defined regarding the associated compressibility factor for Abel–Noble law (1) and Van-der-Waals law (2) (with a the cohesion pressure and b the molar co-volume):

$$Z_{AN} = 1 + \frac{pb}{RT} \tag{1}$$

$$Z_{VdW} = 1 + \frac{pb}{RT} - \frac{a}{vRT} + \frac{ab}{v^2RT} \tag{2}$$

The compressibility factor issued from Abel–Noble EOS is pressure dependent whereas Van-der-Waals and Hemmes EOS ones are pressure and volume dependent. These dependences are carried by a couple of thermodynamic parameters of hydrogen: molar co-volume and cohesion pressure. The molar co-volume represents the intrinsic volume occupied by 1 mol of gas. For low pressures, this volume can be neglected compared to the effective volume available within a cavity which leads to the ideal gas model. In parallel, the cohesion pressure quantifies the attractive–repulsive interactions between the molecules. For low temperatures, the velocity of molecules is drastically decreased which promotes this effect. But for high temperature, such phenomena are not expected since the behavior of gas tends to be defined by ideal gas model (no intrinsic interactions). So, this parameter is expected to be strongly dependent on temperature. Fig. 1, taken from Ref. [30], illustrates the pressure dependence of hydrogen compressibility factor in a [50 K; 300 K] temperature range. More specifically, this figure shows that the pressure dependence of Z tends to be quasi-linear for temperatures above 200 K, at least until 700 bar. In contrast, for low

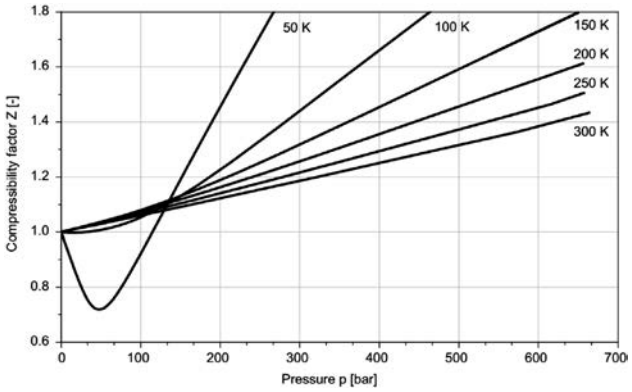

Fig. 1 – Compressibility factor of hydrogen as a function of pressure between 50 K and 300 K [30].

temperatures, a clear minimum and an inflexion point can be distinguished which emphasizes the effects of molecule interactions. This effect is reflected by the cohesion pressure a in both Van-der-Waals and Hemmes EOS. In conclusion, for temperatures higher than 200 K, the molecule interaction forces can be neglected regarding the inertial forces of hydrogen molecules.

An alternative description of hydrogen real gas behavior

Definition of hydrogen fugacity

The proper description of gaseous hydrogen has to be chosen in accordance with application range associated to each EOS. The general intensive expression of an EOS is recalled below (3) (where Z have to be replaced by the correct expression given by the associated real gas model, as stated in the previous section):

$$pv = ZRT \tag{3}$$

Fig. 2 shows the pressure dependence of Z at room temperature. For ideal gas model, Z is constant and is unitary. At room temperature, results issued from Abel–Noble description and Van-der-Waals law are equivalent since the term in $\frac{a}{v^2}$ tends to be close to zero. This figure also puts in evidence that for low pressures, the ideal gas behavior remains accurate.

Knowing that the related fugacity for an Abel–Noble gas is recalled in Ref. [29] and given by (4):

$$f = p \exp\left(\frac{pb}{RT}\right) \tag{4}$$

with b(300 K)=1.584 10^{-5} m^3 mol^{-1}, Fig. 3 represents the evolution of the hydrogen fugacity at room temperature considered as an Abel–Noble gas. This graph points out the nonlinear dependence between the thermodynamic activity (fugacity) and the mechanical behavior of the gas; *i.e.* the stress induced on the surface of the cavity. Considering the Sievert's equilibrium (reminded below in (17)) between hydrogen in solution and gaseous hydrogen within the cavity, the resulting pressure will drastically decrease as compared to the ideal gas case (zero molar co-volume).

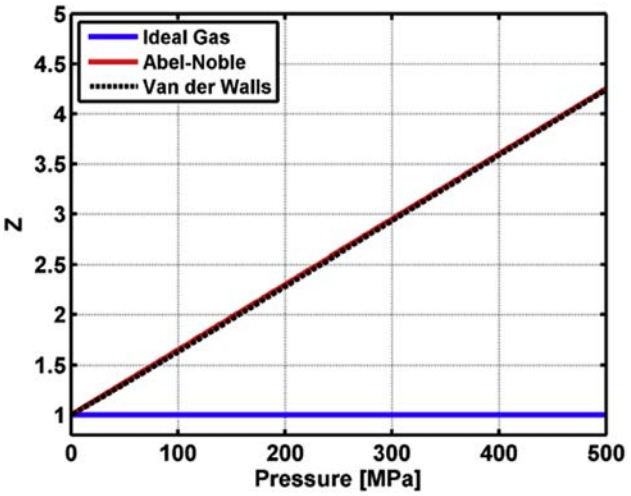

Fig. 2 – Compressibility factor provided by 3 models of gas: ideal gas, Abel–Noble and Van der Walls. This figure clearly underlines that the ideal gas corresponds to the limit case of very low pressures. It also puts in evidence that for high pressures, the ideal gas model cannot be used and both Van der Walls and Abel–Noble equation of states provide equivalent results.

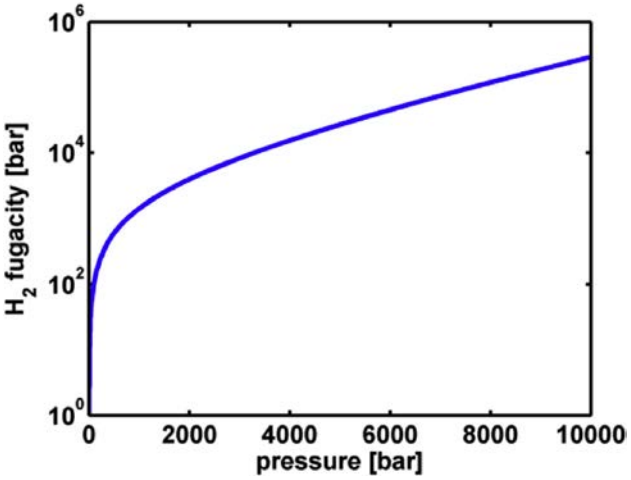

Fig. 3 – Relation between hydrogen fugacity and pressure considered as an Abel–Noble real gas at room temperature.

The point of this first part is to evaluate the cutoff pressure beyond which, the approximation of a linear pressure dependence of Z (as illustrated in Fig. 2 up to 500 MPa i.e. 5000 bars) is not satisfied anymore. To achieve this purpose, the fugacity will be redefined in order ensure an accurate description of hydrogen based on thermodynamic data of hydrogen. The resulting EOS will then be compared to the original Abel–Noble EOS and applied to evaluate the pressure built up within the cavity.

Considering the definition of Gibbs energy, a differential relation (5) between state quantities can be expressed as follows (where V is the considered volume of gas, n the amount of H_2, μ the chemical potential and s the entropy of the system):

$$dG = Vdp - sdT + \mu dn \tag{5}$$

Since the derivatives are continuous, Schwarz theorem leads to symmetric second derivatives (6):

$$\left(\frac{\partial V}{\partial n}\right)_{P,T} = \left(\frac{\partial \mu}{\partial p}\right)_{T,n} \tag{6}$$

By using the general expression of EOS, the dependence of chemical potential on pressure can be quantified (where v represents the molar volume of hydrogen and ρ its inverse) (7):

$$\left(\frac{\partial \mu}{\partial p}\right)_{T,n} = \frac{ZRT}{p} = v = \frac{1}{\rho} \tag{7}$$

This parameter is then integrated (8) between a standard state, noted E^0, and any eligible state designated by E:

$$\int_{E^0}^{E} d\mu = \int_{p^0}^{p} \frac{1}{\rho(p)} dp \tag{8}$$

The chemical potential is then evaluated knowing the pressure evolution of hydrogen density as a function of its pressure. Otherwise, the fugacity of a gas is defined as its thermodynamic activity. The fugacity is therefore linked to a chemical potential defined with respect to a reference which is in this case the standard state and can be expressed by (9):

$$\mu = RT \ln(f) \tag{9}$$

By combining both expressions of the chemical potential (8) and (9), the real gas fugacity can be defined as a function of the pressure (10):

$$f = f^0 exp\left(\frac{1}{RT}\int_{p^0}^{p} \frac{1}{\rho(p)} dp\right) \tag{10}$$

The advantage of this approach is that no prior assumptions on the type of EOS have been done. As a consequence, this expression of fugacity may be directly linked to available thermodynamic data or experimental measurement in order to best fit the real behavior of gaseous hydrogen at any pressure but for temperatures above 200 K (above this threshold temperature, there is no effect of cohesion pressure parameter a). The resulting fugacity therefore reflects the real behavior of hydrogen as accurately as possible.

Refinement of EOS for pressures up to 20 kbar

Thermodynamic data of gaseous hydrogen

The National Institute of Standards and Technology (NIST) have gathered thermodynamic data concerning hydrogen in order to build a comprehensive database containing relevant isothermal and isobaric properties of various entities, including hydrogen. In the considered case, the parameters of interest are the isothermal and isobaric density of the gas. Fig. 4-a) provides the inputs to evaluate hydrogen fugacity at room temperature in the whole pressure range (the hydrogen density is then to be integrated by using the previous expression). Fig. 4-b) compares the fugacity resulting from

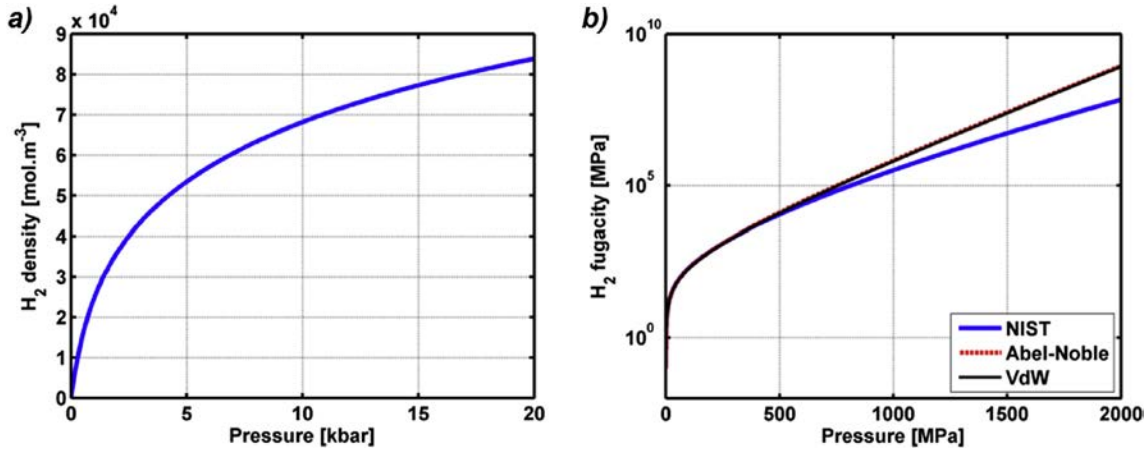

Fig. 4 – a) Evolution of dihydrogen density as a function of pressure at room temperature (isothermal data extracted from NIST open database at 20 °C). b) Comparison of hydrogen fugacity at room temperature for the considered EOS in the pressure range up to 2000 MPa.

Abel–Noble, Van-der-Waals EOS with the data issued from NIST database taken as reference. This figure points out that the cited EOS is valid for pressures up to approximately 3000 bar. Beyond this pressure, the compressibility factor can no longer be considered as linearly dependent on pressure. As a consequence, for a given value of fugacity given by the Sievert's equilibrium an increase of pressure within the cavity is expected as compared to both Abel–Noble and Van-der-Waals EOS.

These observations provide therefore the motivation to refine the description of gaseous hydrogen considered as a real gas for high pressures, beyond 300 MPa. The point is now to provide a refined EOS relying on values extracted from NIST database. As explained in the introduction, the impact of the cohesion pressure may be neglected given the temperature of interest; the refinement therefore consists in the adaptation of molar co-volume of gaseous hydrogen.

Expression of molar co-volume

To determine an accurate description of the pressure and temperature dependence of the molar co-volume b, the identification of the molar volume v is first needed. The preliminary identification of this parameter will be done using the data from NIST database. Fig. 5a presents the evolution of the pv parameter between 0 °C and 750 °C for 5 pressures from 0.8 kbar up to 20 kbar. The evolution is clearly linear. In addition, the curves are all parallel which means that the temperature dependence is pressure independent. Then, the pv factor is assumed to be properly fit by (11) (where α is a constant and B a function of the pressure):

$$pv = \alpha T + B(p) \tag{11}$$

In parallel, Fig. 5b presents the pressure dependence of pv for two temperatures (*i.e.* standard and normal temperatures, respectively 0 °C and 20 °C). It is therefore assumed that the dependence (12) is quadratic (with β, γ constants; the temperature dependence of δ being justified by the parallel but not coincident curves of pv in Fig. 5b):

$$pv = \beta p^2 + \gamma p + \delta_T \tag{12}$$

Then, the different parameters are determined for both temperatures. The fit have been performed by successively determining all the parameters and comparing the results to some values. After several iterations and knowing that at standard state (given by 298.15 K and 1.01325 bar) $b^\circ = 1.4598\ 10^{-5} m^3\ mol^{-1}$, v could be expressed as follows (13):

$$v = \frac{RT}{p} + \beta p + b^0 \tag{13}$$

With $\beta = -1.955.10^{-15}\ m^3\ mol^{-1}\ Pa^{-1}$ (with $r^2 = 0.9996$).

Then, considering that $Z = 1 + \frac{pb}{RT}$ and $Z = \frac{pv}{RT}$, the expression (14) of b could be determined:

$$b = b^0 - 1.955.10^{-15} p \tag{14}$$

In contrast, the regular Abel–Noble description does not take into account the pressure dependency of b; this parameter is therefore taken equal to $1.584\ 10^{-5}\ m^3\ mol^{-1}$ for any values of the pressure.

In other words, the compressibility factor (15) is quadratic regarding the pressure variation:

$$Z = 1 + \frac{pb^0}{RT} - 1.955.10^{-15}\frac{p^2}{RT} \tag{15}$$

Fig. 6 represents the evolution of the NIST standard and refined compressibility factors as a function of pressure in the considered range and compared to the regular Abel–Noble description. The above demonstrated expression and concomitant plot of NIST refined compressibility factor will further be considered as reliable and accurate description of hydrogen real gas.

The first part of the present paper has proposed a refined description of gaseous hydrogen in manufacturing process condition. Under these conditions, the use of more refined expression like Van-der-Waals or Hemmes EOS is unnecessary since manufacturing temperatures are always higher

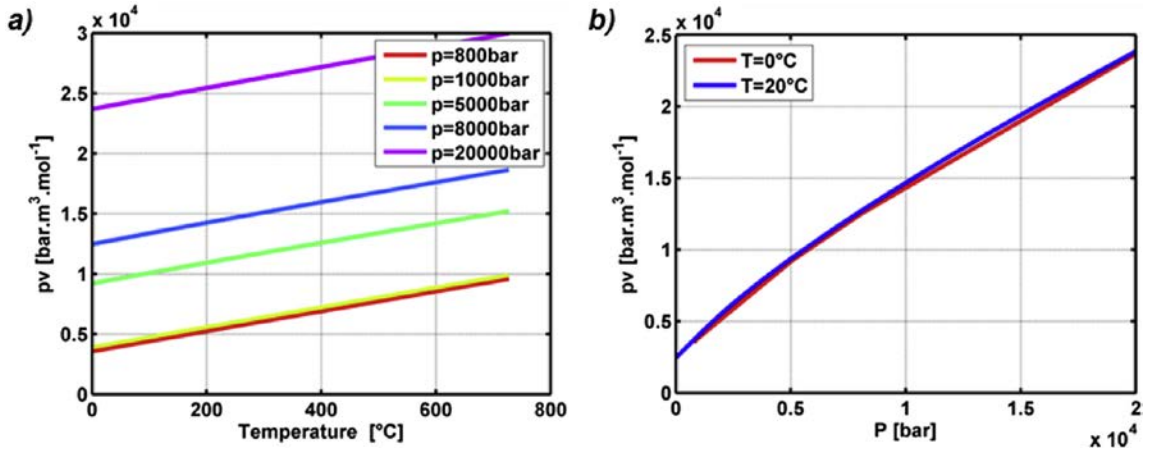

Fig. 5 – Identification of the pv parameter as a function of temperature (a) and pressure (b); fit using a pressure dependent quadratic expression and a linear temperature dependence.

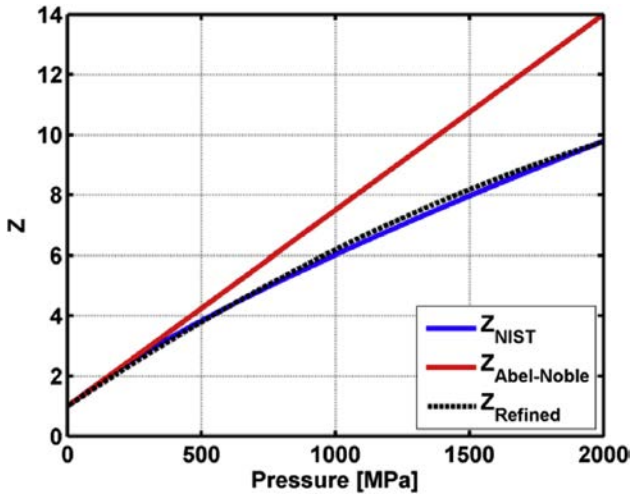

Fig. 6 – NIST standard and refined compressibility factors defined with a pressure dependant molar covolume and compared to the initial Abel–Noble expression.

than 200 K. However, the proposed NIST refined compressibility factor which derives from Abel–Noble model is certainly necessary to ensure accurate pressure calculations. This formulation is now to be applied to evaluate the internal pressure within a cavity that can be reached in heavy components during heat treatment.

Pressure build-up in pre-existing cavities during heat treatment

Recall of a heterogeneous microstructure of 16-20MND5 steel

The component of interest is a lower shell of a steam generator, specific equipment at the junction between primary and secondary circuits in pressurized water reactor (PWR). Different types of segregation are observable in the component at micro, meso and macroscales. These segregations are issued from solidification process; in which solutal and thermal convection generate a heterogeneous composition of the alloy. These composition heterogeneities induce a strong space dependence of diffusion parameters (diffusivity and solubility) and allotropic transformations. Fig. 7 shows (a) the aforementioned heterogeneities at microscopic scale, (b) the presence of decohesions in the MnS vicinity and (c) the resulting bainitic microstructure of the alloy. The alloy of a nominal composition is called matrix. The areas of solute enrichment at a mesoscale are called segregation bands (SB). Note that carbon segregation at a macroscale (between the top and the bottom of the ingot) is not considered in this approach. As a consequence, a dynamic redistribution of hydrogen between the different phases (matrix and segregation band) occurs during heat treatment. This redistribution is driven by the evolution of solubility within both phases as previously described in Ref. [26].

Physical model and numerical implementation

A physical model of hydrogen redistribution in a heterogeneous material as a function of temperature based on diffusion equation and taking into account solubility and diffusivity variations with temperature as well as composition dependent phase transformation has been proposed in our previous paper [26] in order to estimate both the redistribution of hydrogen between the matrix and the segregation band and to calculate pressure increase in the cavity hold at 200 °C, i.e. before hydrogen outgassing in a manufacturing process. All initial and boundary conditions have been extensively discussed, however in this previous work hydrogen was treated as an ideal gas, therefore fugacity in Sieverts law was directly replaced by pressure which was fully justified by a minimum temperature of 200 °C *i.e.* well above room temperature. In the following part we will use this model together with the redefined fugacity of hydrogen as demonstrated above and an updated geometry of the simulation box.

The assessment of internal pressure within the cavity will be done at a component scale using two simulation boxes as illustrated in Fig. 8. It has been assumed that, in a 200–240 mm thick shell, only the hydrogen located in the core will

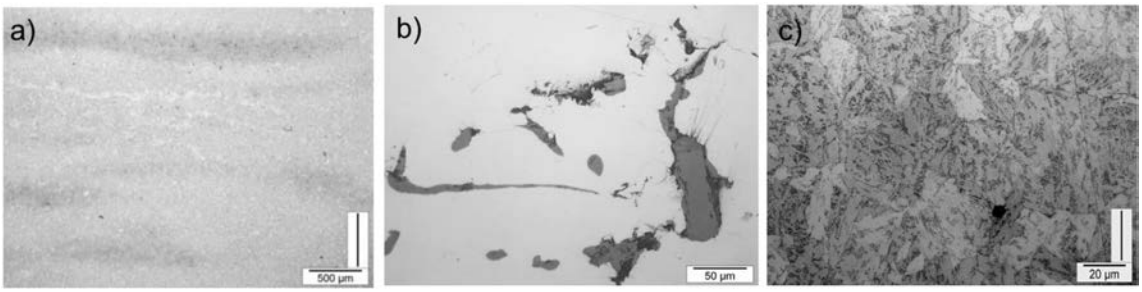

Fig. 7 – Observations of the microstructure of the alloy: (a) heterogeneous composition in which segregated bands are revealed by Nital attack, (b) non-coherent cluster of MnS, (c) bainitic acicular microstructure.

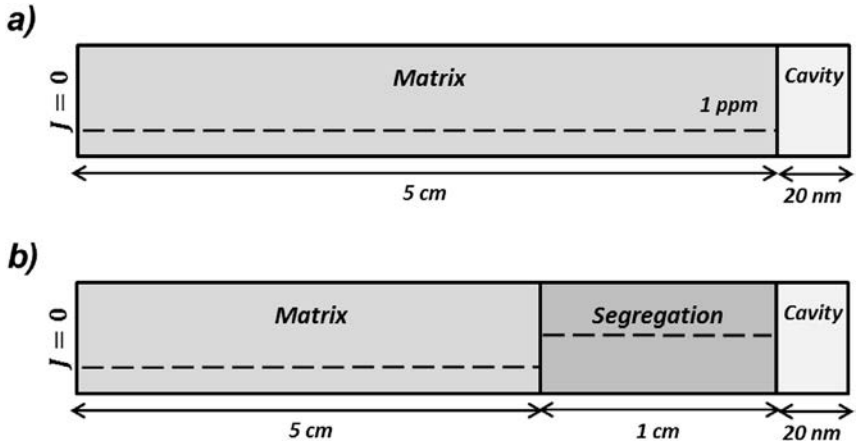

Fig. 8 – Schematic representation of two simulation boxes. Simulations are carried out at a component scale to take into account kinetic effects of hydrogen outgassing. a) H_2 desorption in a nanometric cavity located in bulk. b) H_2 desorption in a nanometric cavity located in the vicinity of a segregation band.

contribute to the pressure build-up since the hydrogen located near the inner and outer surfaces would outgas during the process. Together with the symmetric boundary condition applied at mid thickness a 5–6 cm wide simulation box is obtained. A zero flux condition at the left side has been considered to isolate the hydrogen outgassed through the external surface from the hydrogen diffusing towards the cavity. The first simulation consists in a 5 cm wide homogeneous simulation box located nearby a 20 nm thick cavity which corresponds to the matrix-inclusion non-coherent interface (*e.g.* MnS, see Fig. 7b). This interface is assumed to be an initially empty cavity (see Fig. 8a). The decohesion of the non-metallic inclusion from the alloy can be induced either by forging or by thermal shrinking of the steel during cooling [37]. The second simulation box represents a heterogeneous alloy composed of a matrix, a segregation band and a cavity. The point of this second case study, illustrated in Fig. 8b, is to evaluate the interactions between the localization of reticular hydrogen and the presence of segregations which, owing to the difference of solubility, are more likely to uptake hydrogen in solution. These two cases are schematized on Fig. 8. The relevance of the refined EOS presented in the first part of the paper will then be highlighted by comparing results issued from the regular Abel–Noble law.

The differences between the inputs parameters considered in the following simulations are synthetized by Table 1.

In order to conduct these simulations, the diffusive properties of the heterogeneous alloy and related data have been taken from Ref. [26]. Based on process guideline of such components, a 30 °C h^{-1} cooling rate was applied and the initial amount of hydrogen was taken to be equal to 1 wt ppm corresponding to the maximal admissible concentration of hydrogen usually encountered during such processes.

Hydrogen outgassing from the matrix to the cavity: effect of the refined EOS on the equilibrium pressure

Two calculations using a 5 cm simulation box have been performed to emphasize the effect of the refined EOS on the equilibrium pressure in the cavity. Fig. 9 provides the results related to a regular Abel–Noble EOS with a constant covolume. The first plot (a) shows the evolution of concentration profile in the matrix during the cooling down to the room temperature and subsequent evolution at 20 °C. The initial and steady states are represented with solid curves whereas the transient states are plotted with dashed curves. The second plot represents the temporal evolution of pressure evolution within the cavity. Three stages can be distinguished

Table 1 – Comparison of input parameters involved in the simulations.

	Simulation 1a	Simulation 1b	Simulation 2a	Simulation 2b
Nature of the material	Homogeneous	Homogeneous	Heterogeneous	Heterogeneous
Dimensions of the simulation box (MAT/SB)	5 cm/–	5 cm/–	5 cm/1 cm	5 cm/1 cm
Considered Abel-Noble EOS	Regular	Refined	Regular	Refined

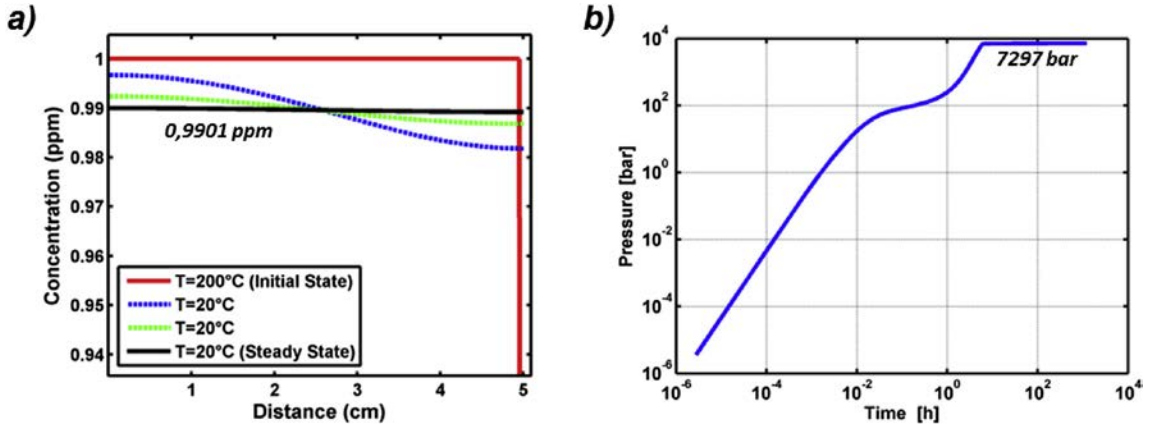

Fig. 9 – Simulation 1a using regular Abel–Noble EOS: Diffusion and outgassing of internal hydrogen from the matrix to the cavity during a slow cooling (30 °C h^{-1}) from 200 °C to 20 °C and subsequent slow outgassing. a) Concentration profile of hydrogen in the matrix at various temperatures from initial state (200 °C, in red solid line) to final state (20°, in black solid line). The transients are given in dashed lines. b) Evolution of pressure within the cavity during the simulation considering an Abel–Noble EOS. (For interpretation of the references to color in this figure legend, the reader is referred to the web version of this article.)

during the pressurization of the cavity. First, a strong exponential increase occurs due to the fact that the cavity is initially empty. It results in a close-to-zero concentration at the solid–gas interface according to Sievert's thermodynamic equilibrium and consequently a maximized desorption flux across the interface. Then, desorption slows down due to hydrogen lack close to the interface and reaccelerate once hydrogen from the bulk reaches the interface. The final plateau corresponds to the slow increase of pressure until the homogenization of the concentration all along the 5 cm thick solid and reaching the steady state. It also could be noted that a significant pressure of 7100 bars is already reached within the 10 first hours and the hundred following hours lead to an increase of approximately 200 bars. Concerning the evolution of the amount of hydrogen remaining in solution in the matrix, the amount transferred to the cavity is negligible since it represents approximately 1% of the initial amount in the matrix.

Fig. 10 shows the results obtained on the same simulation box with identical initial conditions but considering now the refined EOS. The graph plotted in Fig. 10-a) represents hydrogen concentration profiles while graphs in (b) and (c) represent the time dependence of hydrogen pressure. The inputs of this couple of simulation being close, the observations and trends concerning general evolution of the system stated for the previous simulation remain valid for this case. The final pressure within the cavity is now increased up to 8632 bars. The modification of the equation of state results in a significant increase of the calculated pressure within the cavity, by 1335 bar. In parallel, due to the fact that the fugacity calculated from the refined EOS is lower as compared to Abel–Noble law, the interfacial concentration induced by Sievert's equilibrium is decreased which slightly reduces the total amount of hydrogen in the matrix down to 1.2% of the initial amount. As compared to the previous simulation based on the regular Abel–Noble EOS, the fugacity has decreased by 1800 bar (from 837,380 bar to 835,580 bar). As a consequence, the interfacial concentration in the simulation presented on Fig. 9 is 0.9901 ppm while in the second simulation involving refined EOS and given by Fig. 10, the concentration is 0.9884 ppm. These parameters lead to different amounts of hydrogen within the cavity. An increase of $2.78.10^{-8}$ mol is observable in the refined EOS simulation as compared to the regular Abel–Noble law (respectively $1.51.10^{-7}$ mol and $1.23.10^{-7}$ mol). It is important to underline that even if the difference in interfacial concentration is very small, the simulation using the refined NIST law results in a significant increase of pressure and hydrogen uptake in the cavity.

The substantial pressure raise (8632 bars, i.e. 863 MPa instead of 7297 bars, i.e. 730 MPa) induced by this refinement and its consequences will further be discussed.

Effects of microsegregations on equilibrium pressure

The simulation box used in this section corresponds to a generalized case of a heterogeneous alloy composed of

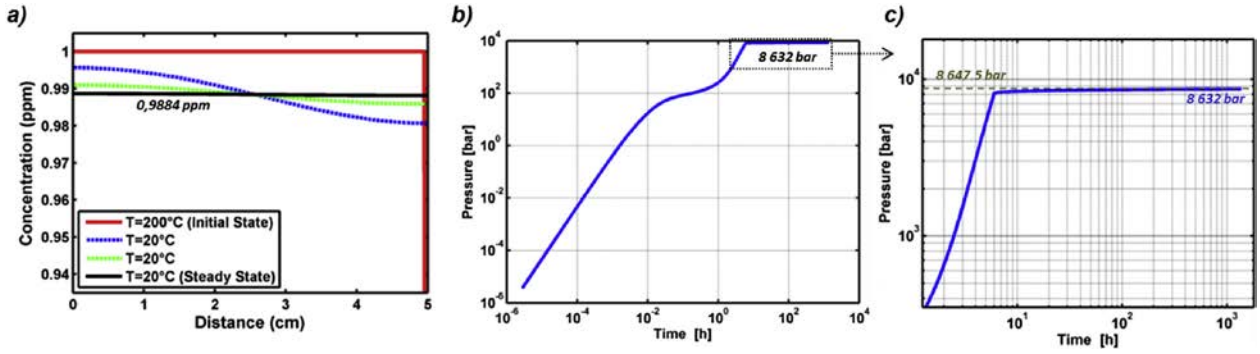

Fig. 10 – Simulation 1b using refined EOS: Diffusion and outgassing of internal hydrogen from the matrix to the cavity during a slow cooling (30 °C h^{-1}) from 200 °C to 20 °C and subsequent outgassing. a) Concentration profile of hydrogen in the matrix at various temperatures from initial state (200 °C, in red solid line) to final state (20°, in black solid line). The transients are given in dashed lines. b) Evolution of pressure within the cavity during the simulation considering the refined EOS. c) Focus on the slow pressure build-up until reaching the target equilibrium pressure calculated by mass balance represented by the dashed line. (For interpretation of the references to color in this figure legend, the reader is referred to the web version of this article.)

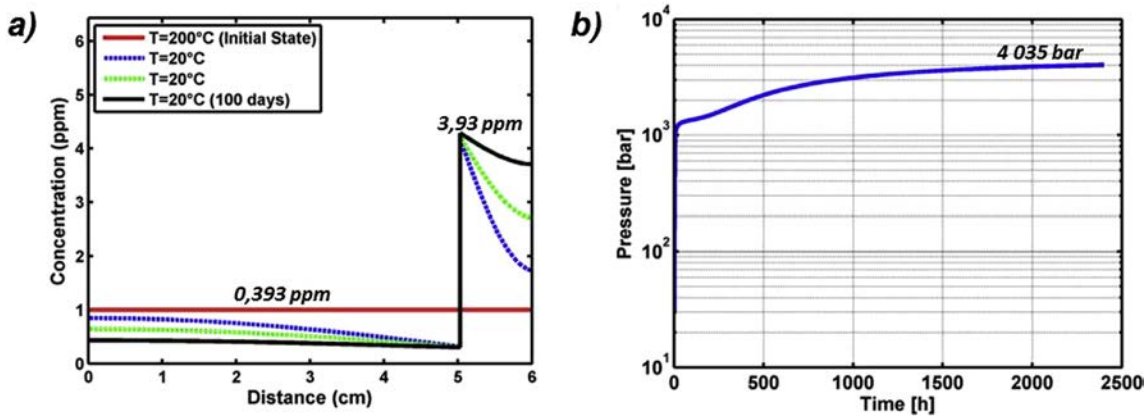

Fig. 11 – Simulation 2a using a regular Abel–Noble EOS: Diffusion and outgassing of internal hydrogen in a heterogeneous alloy, modeled as matrix-segregation band-cavity, during a slow cooling (30 °C h^{-1}) from 200 °C down to 20 °C and subsequent very long outgassing at 20 °C towards equilibrium. a) Concentration profile of hydrogen in the solid at various temperatures from initial state (200 °C, in red solid line) to final state (20 °C and 100 simulated days, in black solid curve). The transients are given in dashed lines. Concentrations are given at mid thickness of each phase; interfacial concentrations are respectively 0.30 ppm and 4.3 ppm for matrix and segregation. b) Evolution of pressure within the cavity during the 100 days simulation considering an Abel–Noble EOS. (For interpretation of the references to color in this figure legend, the reader is referred to the web version of this article.)

matrix, segregation band and cavity. Two simulations involving respectively regular Abel–Noble formulation and the refined EOS are presented below.

The results of the first simulation, based on Abel–Noble EOS, are given Fig. 11. The first plot (a) shows the evolution of hydrogen concentration during the cooling at 30 °C h^{-1} down to 20 °C (in 6 h) and subsequent maintain at 20 °C for almost 100 days (2394 h). The hydrogen concentration profile, initially uniform at 1 wt ppm and continuous across the two areas, evolves into a discontinuous profile, the discontinuity being located at the matrix-segregation band interface. In addition, a localization of hydrogen is observable during the process of cooling since hydrogen solubility is higher in the segregation band than in the matrix by a factor 14.5 at room temperature. Then, transient curves underline the high gradient generated by the matrix-segregation interface which enhances the mass diffusion flux as defined by Fick's law. The second graph represents the evolution of pressure within the cavity. As compared to previous cases, the same global behavior is observable. Two main differences concern the final pressure and the kinetics of desorption. Although the simulation has been performed on an extended domain, which therefore contains a greater amount of hydrogen, the final pressure is lower than in the previously analyzed matrix-cavity simulation box. That major difference can be easily understood if we recall that segregation band is characterized by a 14.5 higher solubility and consequently a significant amount of hydrogen will be stored in the segregation band as illustrated in Fig. 11-a) while the matrix will eventually contain less than 0.4 wt ppm. Moreover, at equilibrium, ^{c} ratio must be constant across

the solid part of simulation box and recalling that hydrogen fugacity is proportional to $\left(\frac{c}{S}\right)^2$ we easily understand that the final pressure is much lower in this case, The second difference concerns the kinetics of hydrogen diffusion and outgassing which remains similar in spite of the slightly higher dimensions of the simulation box and the pronounced gradient of hydrogen concentration within the segregation band which promotes the desorption flux. It is clear that in this simulation equilibrium has not been reached after a period of 100 days. The final calculated pressure of 4035 bars is lower than the equilibrium pressure that can be obtained from mass balance equation, see discussion below.

The second case is reported in Fig. 12. This simulation based on the refined EOS proves that the pressure build-up in the cavity is enhanced with no notable influence of desorption kinetics as compared to the reference Abel–Noble gas description. Qualitatively, similar conclusions can be given with respect to hydrogen diffusion from the matrix to the segregation band due to its much higher solubility. Again the system evolves towards equilibrium with the maximum calculated pressure of 4472 bars which represents an increase of 437 bars as compared to the simulation based on Abel–Noble EOS.

Substituting Abel–Noble EOS by a refined NIST EOS in above presented simulations has always resulted in an increase of a final pressure within the cavity. The results and impacts will now be discussed with respect to the industrial context.

Discussion

Mass balance verification

In all simulations, the refinement of real gas description has resulted in a substantial increase of the pressure build-up due to the modified fugacity – pressure relation. The gas description is a key point to provide an accurate assessment of the peak pressure reachable within the cavity after desorption of internal hydrogen. This pressure has been hereon presented via simulation since a transient analysis is needed to put in evidence kinetic effects. But the equilibria are only governed by a couple of parameters: hydrogen solubility and thermodynamic properties of gas. The steady state could therefore be evaluated analytically by considering the mass balance with a constraint on hydrogen desorption. For clarity of expressions, we consider below the case of our first simulation box composed of a matrix and a cavity (the case of matrix-segregation_band-cavity requires one additional equation of continuity for c/S ratio at the matrix/segregation band interface and would lead to the same conclusions).

The balance of mass between the initial state, where hydrogen is located only within the matrix (referred by 0 superscript) and the steady state, where hydrogen is redistributed among matrix and cavity (referred by f superscript) can be expressed by (16):

$$n^0_{MAT} = n^f_{MAT} + n^f_{HIC} \tag{16}$$

Then, the Sievert equilibrium is expressed by (17), S being the solubility of hydrogen in the alloy.

$$c = S\sqrt{f_{H_2}} \tag{17}$$

Steady state, or thermodynamic equilibrium, consists in a minimization of chemical potential and is illustrated in this case by a flat concentration profile. The balance of mass can be expressed by (18):

$$c^0 V_{MAT} = V_{MAT} S\sqrt{f_{H_2}} + \frac{pV_{HIC}}{ZRT} \tag{18}$$

Knowing the relation between fugacity and pressure, the pressure at thermodynamic equilibrium can be determined.

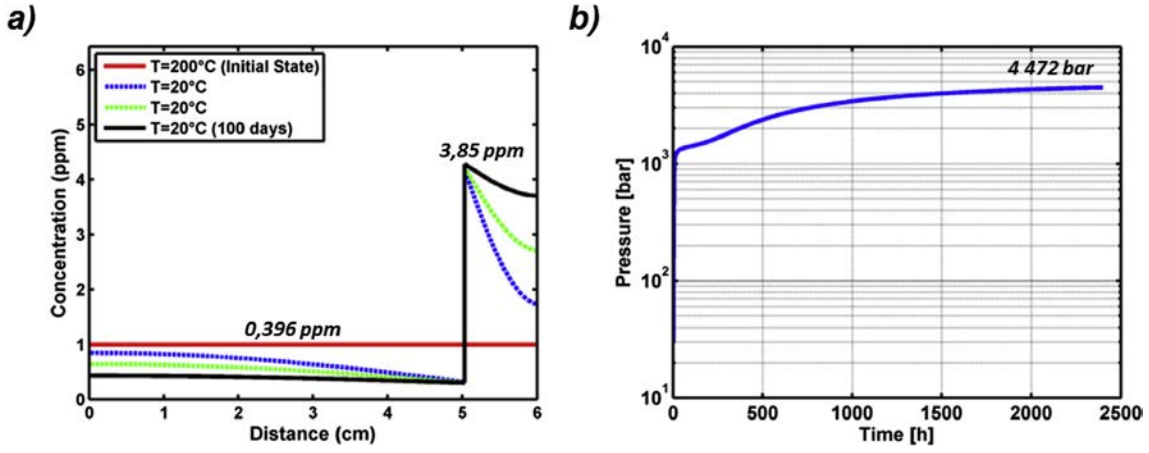

Fig. 12 – Simulation 2b using the refined EOS based on NIST open database: Diffusion and outgassing of internal hydrogen in a heterogeneous alloy, modeled as matrix segregation band cavity, during a slow cooling (30 °C h^{-1}) from 200 °C to 20 °C and subsequent very long outgassing at 20 °C towards equilibrium. a) Concentration profiles of hydrogen in the solid at various temperatures from initial state (200 °C, in red solid line) to final state (20 °C and 100 simulated days, in black solid curve). The transients are given in dashed lines. Concentrations are given at mid thickness of each phase; interfacial concentrations are respectively 0.30 ppm and 4.3 ppm for matrix and segregation. b) Evolution of pressure within the cavity during the 100 days simulation considering the refined EOS (an increase of 437 bars is noticed as compared to the Abel–Noble EOS. (For interpretation of the references to color in this figure legend, the reader is referred to the web version of this article.)

At this point, gaseous hydrogen is described using the refined expression (19) of compressibility factor corresponding to the general case in the considered temperature range:

$$Z = 1 + \frac{pb^0}{RT} - 1.955\ 10^{-15}\frac{p^2}{RT} \tag{19}$$

The final pressure can be numerically evaluated by calculating the zeros of the following function g (20):

$$g(p) = V_{MAT}S\sqrt{p\exp\left(\frac{pb(p)}{RT}\right)} + 2\ \frac{pV_{HIC}}{RT + pb^0 + \beta p^2} - c^0V_{MAT} \tag{20}$$

The value of this pressure was calculated for different EOS by replacing the expression of molar co-volume in the previous expression. For Abel–Noble model description the molar co-volume at 300 K is 1.584 10^{-5} m^3 mol^{-1} (with no pressure dependency). For ideal gas, no intrinsic volume is considered for hydrogen molecules. Final pressures were calculated for these gas models and the values are 8647.5 bars for the refined EOS, 7305.8 bars for the Abel–Noble model and finally 141,120 bars for the ideal gas model; which has to be considered as unrealistic regarding the mechanical properties of the alloy. The above calculated equilibrium pressures for Abel–Noble EOS and modified NIST EOS are slightly higher than the final values obtained in our kinetic simulations (respectively 7297 bars in Fig. 9-b) and 8632 bars in Fig. 10-b)) because these kinetic calculations were stopped after approximately 600 h and consequently equilibrium has not been reached. It is also worth noting that the numerical accuracy of hydrogen pressure inside the cavity, as calculated with the present model, is excellent with an absolute error of only 10^{-8} bar.

Concerning the heterogeneous case, equilibrium pressures were also calculated using a similar approach as introduced above. Briefly, by noticing that the ratio of compositions at the matrix-segregation band interface is equal to the ratio of solubilities between the two compositions, and considering that the concentration profile is step shaped (*i.e.* flat in each phases taken separately), the final pressure could therefore be calculated using the mass balance equation and the Sievert's equilibrium constraint. The values of equilibrium pressures were again slightly above the ones presented in Fig. 11-b) and Fig. 12-b) and consequently the presented simulations have then been indirectly validated by this method.

Effect of hydrogen solubility on equilibrium pressure

Our calculations have allowed determining the maximum internal pressure reached in cavities. These results strongly depend on values of solubility at room temperature; which differ between the matrix and the segregation band, being respectively 1.081 10^{-3} ppm $bar^{0.5}$ and 1.57 10^{-2} ppm $bar^{0.5}$. According to Sievert's law, pressure increases with solubility decrease which leads to different steady state pressure depending on the position of the cavity in the component. In other words, a cavity localized in the matrix would have a greater pressure than a cavity located in the segregation band. This statement is verified for a cavity close to either the matrix or the segregation band but wouldn't be true for a cavity located between the matrix and the segregation band, i.e. in contact with a matrix and with a segregation band in the same time. This point can be explained by considering the two Sievert equilibria respectively at matrix-cavity interface and at segregation band-cavity interface. Without going into a detailed explanation it can be concluded that the final pressure in such a heterogeneous media will result from two Sieverts equilibria at both interfaces with hydrogen transport through the cavity as long as necessary to satisfy both equilibria in accordance with the considered thickness of each phase (determining thereby the amount of hydrogen and its redistribution). As a general rule, for a cavity embedded in a given area of a heterogeneous alloy, the lower the solubility of the material in contact with a cavity is the higher the equilibrium pressure is.

Consequence of a non-linear fugacity-pressure dependence

Another interesting point resulting from the non-linear nature of the fugacity-pressure dependence is the peculiar relation between the pressure and the amount of hydrogen within the cavity. The amount of hydrogen is expressed in the case of a refined NIST EOS by (21):

$$n = \frac{pV}{RT + pb^0 - 1.955\ 10^{-15}p^2} \tag{21}$$

Considering a pressure of 8000 bar and a volume of 2.00 10^{-12} m^3 (*i.e.* 1 cm^2 "penny-shaped" thin cavity of 20 nm), the corresponding amount of hydrogen is 1.24 10^{-7} mol for refined description and 1.06 10^{-7} mol for Abel–Noble model. These values, for a pressure of 10,000 bar will be respectively 1.33 10^{-7} mol and 1.09 10^{-7} mol. Consequently, a pressure increase of 25% requires an increase regarding the amount of hydrogen of 6.6% in case of the refined NIST EOS and only 3.3% for Abel–Noble EOS. The uptake of hydrogen generated by the proposed EOS is therefore twice as high as the uptake issued from v gas description.

Conclusion

A refined EOS based on Abel–Noble model has been proposed to accurately evaluate the equilibrium pressure within internal cavities up to 20 kbar. This alternative approach is based on the fugacity pressure dependence deduced from NIST database, valid up to 20,000 bar and for temperatures above 200 K. The quadratic fugacity-pressure dependence results in a decreased fugacity at high pressure as compared to the reference Abel–Noble description. This new EOS for hydrogen is completely based on NIST thermodynamic datasets.

The updated fugacity-pressure dependence implies a decreased chemical activity of gaseous hydrogen for extreme pressures, and consequently, for a given fugacity, resulting from Sievert's equilibrium; the corresponding pressure is higher than that calculated from that Abel–Noble EOS. This increase in pressure has been calculated to be of the order of 10% for a matrix/cavity interface and 20% for segregation-band cavity interface. This refined NIST EOS was introduced to our previously developed numerical code to calculate the kinetics of hydrogen transfer from the bulk to the cavity during outgassing. Two simulation boxes, representative of an industrial component have been defined and clearly indicate

that values very close to equilibrium can be obtained following slow cooling rate down to room temperature and subsequent maintain for a period of going from approximately 600 h up to 100 days. The validity of this kinetic calculation was checked through mass balance approach. The final equilibrium pressure depends on the position of the cavity within the material: if in contact with a segregation band (high hydrogen solubility) this pressure is of the order of 4500 bars and if in contact with a matrix (low hydrogen solubility) this pressure is of the order of 8650 bars.

REFERENCES

[1] Coudreuse L. Fragilisation par l'hydrogène et corrosion sous contrainte ; Corrosion sous contrainte – phénoménologie et mécanismes. In: Desjardins D, Oltra R, editors; 1992. p. 397–424. Les Editions de Physique.

[2] Kirchheim R. Reducing grain boundary, dislocation line and vacancy formation energies by solute segregation. I. Theoretical background. Acta Mater 2007;55(15):5129–38.

[3] Kirchheim R. Reducing grain boundary, dislocation line and vacancy formation energies by solute segregation. II. Experimental evidence and consequences. Acta Mater 2007;55(15):5139–48.

[4] Kirchheim R. Revisiting hydrogen embrittlement models and hydrogen-induced homogeneous nucleation of dislocations. Scr Mater 2010;62(2):67–70.

[5] Troiano AR. The role of hydrogen and other interstitials in the mechanical behavior of metals. Trans ASM 1960;52:54.

[6] Petch NJ, Stables P. Delayed fracture of metals under static load. Nature 1952;169:842–3.

[7] Ruel F, Saedlou S, Le Manchet S, Lojewski C, Wolski K. The influence of temperature and pH on the EAC behavior of the UNS(1) S32304 lean duplex stainless steel. In: Corrosion/14 conference paper, NACE international; 2014.

[8] Kane RD, Cayard MS. Roles of H_2S in the behavior of engineering alloys: a review of literature and experience. In: Corrosion/98, paper n°274, NACE international; 1998.

[9] Chen Y, Zheng S, Zhou J, Wang P, Chen L, Qi Y. Influence of H2S interaction with prestrain on the mechanical properties of high-strength X80 steel. Int J Hydrogen Energy 2016;41:pp.10412–10420.

[10] Wang P, Wang J, Zheng S, Qi Y, Xiong M, Zheng Y. Effect of H_2S/CO_2 partial pressure ratio on the tensile properties of X80 pipeline steel. Int J Hydrogen Energy 2015;40:pp.11925–11930.

[11] Ren X, Chu W, Li J, Su Y, Qiao L. The effects of inclusions and second phase particles on hydrogen-induced blistering in iron. Mater Chem Phys 2008;107:231–5.

[12] Dunne DP, Hejazi D, Saleh AA, Haq AJ, Calka A, Pereloma EV. Investigation of the effect of electrolytic hydrogen charging of X70 steel : I. The effect of microstructure on hydrogen-induced cold cracking and blistering. Int J Hydrogen Energy 2016;41:12411–23.

[13] Petch NJ. The lowering of fracture-stress due to surface adsorption. Philos Mag 1956;1(4):331–7.

[14] Matsuoka S, Matsuo T, Homma N, Murakami Y. Effect of hydrogen and prestrain on tensile properties of carbon steel SGP (0.078 C-0.012 Si -0.35 Mn, mass %) for 0.1 MPa hydrogen pipelines. Trans JSME A 2008;74(744):1164–73.

[15] Matsuo T, Matsuoka S, Murakami Y. Fatigue crack growth properties of quenched and tempered Cr-Mo steel in 0.7 MPa hydrogen gas. In: ECF 18 conference proceedings; 2010.

[16] C.A. Zapffe et al. Hydrogen flakes and shatter cracks. Met Alloys, AA00722827; 12: 145–151.

[17] Pressouyre GM. Implication industrielles de I 'hydrogène. In: 3e Congrès International Hydroene et Materiaux; 1982. p. 1–15.

[18] Safety case report Doel 3–reactor pressure vessel assessment. Electrabel; 2012.

[19] Wampler WR, Doerner RP. The influence of displacement damage on deuterium retention in tungsten exposed to plasma. Nucl Fusion 2009;49(11):115023.

[20] Furuseth S, Kjekshus A. On the properties of α-MnS and MnS2. ACTA Chem Scand 1965;19:1405–10.

[21] Taylor RE. CINDAS data series on materials properties. Therm Expansion Solids 1998;1–4. ASM International.

[22] Traidia A, et al. Model of parameters controlling resistance of pipeline steels to hydrogen Induced Cracking. Corrosion 2013;70:87–94.

[23] Traidia A, et al. An effective finite element model for the precipitation of hydrogen induced cracking in steel pipeline. Int J Hydrogen Energy 2012;37:16214–30.

[24] Kolasinski RD, et al. A continuum-scale model of hydrogen precipitate growth in tungsten plasma-facing materials. J Nucl Mater 2011;415:S676–9.

[25] Tiegel MC, et al. Crack and blister initiation and growth in the purified iron due to hydrogen loading. Acta Mater 2016;115:24–34.

[26] Sezgin J-G, et al. Modelling of hydrogen redistribution in a heterogeneous alloy and simulation of cooling down to 200 °C. Int J Hydrogen Energy 2017.

[27] Du XS, Cao WB, Wang CD, Li SJ, Zhao JY. Effects of microstructures and inclusions on hydrogen-induced cracking and blistering of A537 steel. Mater Sci Eng A 2015;642:181–6.

[28] Atkins PW, Jones LL. Chemie-einfach alles. Wiley-VCH; 2006.

[29] San Marchi C, Somerday BP, Robinson SL. Permeability, solubility and diffusivity of hydrogen isotopes in stainless steels in gas pressures. Int J Hydrogen Energy 2007;32:100–16.

[30] Klell M. In: Hirscher M, editor. Chapter 1 : storage of hydrogen in the pure form. Handbook of hydrogen storage. WILEY-VCH; 2010.

[31] Johnston IA. The Noble-Abel equation of state: thermodynamic derivations for ballistic modelling. Australian Department of Defense; 2005. Report DSTO-TN-0670.

[32] Hemmes H, et al. Thermodynamic properties of hydrogen between 100 and 1000K at pressures up to 1Mbar. Physica 1986;139 & 140B:116–8.

[33] E.J. Pickering, ISIJ international, Vol. 53 (2013), No. 6, p 935.

[34] Naudin C, Frund JM, Pineau A. Intergranular fracture stress and phosphorus grain boundary segregation of a Mn-Ni-Mo steel. Scr Mater 1999;40(9):1013–9.

[35] L.Bedel et al. Comparison des aciers de cuve utilisés dans les programmes Rupther et Krakatoa. Technical Note DEM n°98/15, CEA Grenoble.

[36] Campbell J. Complete casting handbook : metal casting processes, techniques and design. Elsevier Science; 2011. p. 246–53.

[37] Juvoven P. Effects of non-metallic inclusions on fatigue properties of calcium treated steels. University of Helsinki; 2004. PhD Thesis.